

## Supplementary Data of the Results

### “Profiling microglia in a mouse model of Machado-Joseph disease”

by Campos et al., 2022

#### Contents within the present file:

##### 1. Supplementary Figures:

**Suppl. Figure S1.** Confirmation of the high purity of microglia in culture.

**Suppl. Figure S2.** Expression of mutant *ATXN3* in microglia from CMVMJD135 mice at two different time points in culture.

**Suppl. Figure S3.** Microglia expressing *ATXN3* showed a less activated phenotype in response to lipopolysaccharides (LPS) in artificially “aged” primary cultures.

**Suppl. Figure S4.** CMVMJD135 and Wild-Type (WT)-derived microglia showed an increased phagocytic efficiency in the presence of LPS in culture.

**Suppl. Figure S5.** The ramification state of microglia in the pontine nuclei (PN) of the CMVMJD135 mice is similar to those of microglia from WT mice.

**Suppl. Figure S6.** The complexity and shape of microglia in the PN of CMVMJD135 mice are similar to those of microglia from WT mice.

**Suppl. Figure S7.** Microglia in the deep cerebellar nuclei (DCN) of CMVMJD135 mice showed no differences in features relevant to microglia ramification.

**Suppl. Figure S8.** Microglia in the DCN of CMVMJD135 mice showed no changes in the complexity and shape.

**Suppl. Figure S9.** Some parameters associated with microglia ramification were similar between CMVMJD135 and WT mice in the cervical spinal cord (CSC).

**Suppl. Figure S10.** No changes were observed in the parameters related to the complexity of ramifications and with the cylindrical shape of the cells between groups in the CSC.

**Suppl. Figure S11.** Evaluation of microglial enrichment in RNA-sequencing samples.

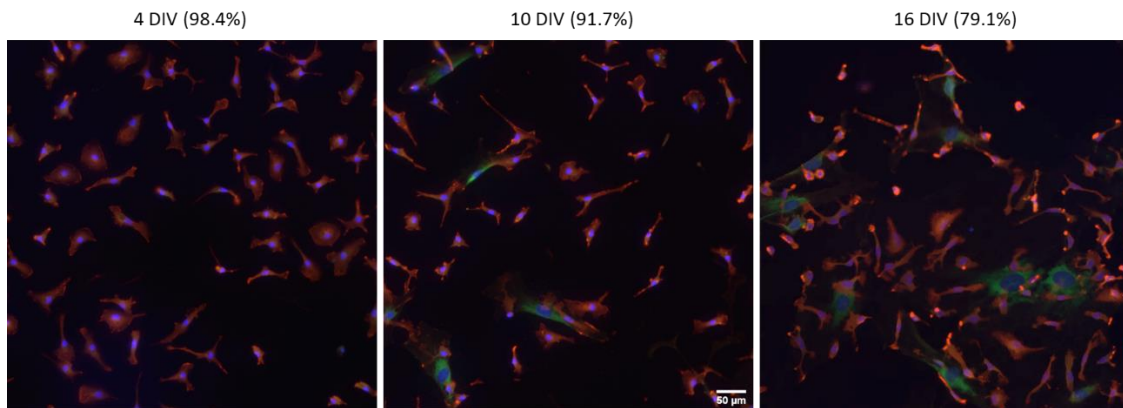
**Suppl. Figure S12.** Differential gene expression between microglia from CMVMJD135 and WT mice.

**Suppl. Figure S13.** Transcriptional changes seen in CMVMJD135 microglia overlap those in Amyotrophic lateral sclerosis (ALS) and Alzheimer disease (AD) mouse models.

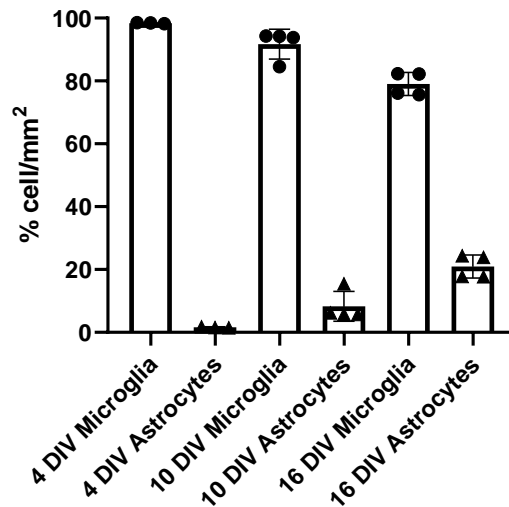
## 2. Supplementary References

### Purity assessment of microglia culture over time

a)

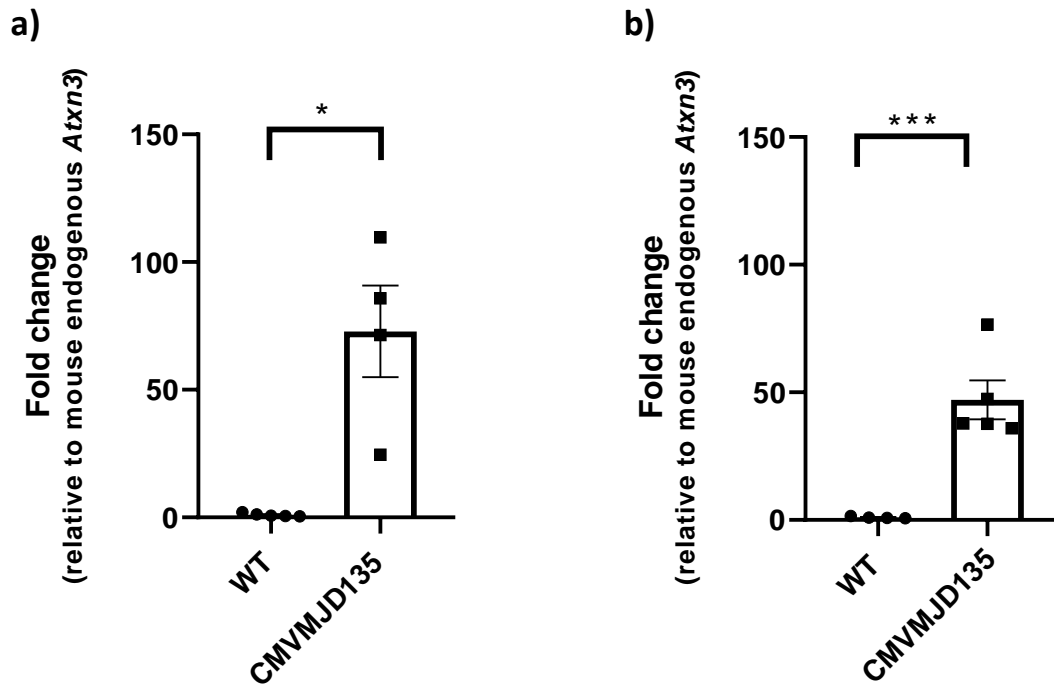


b)



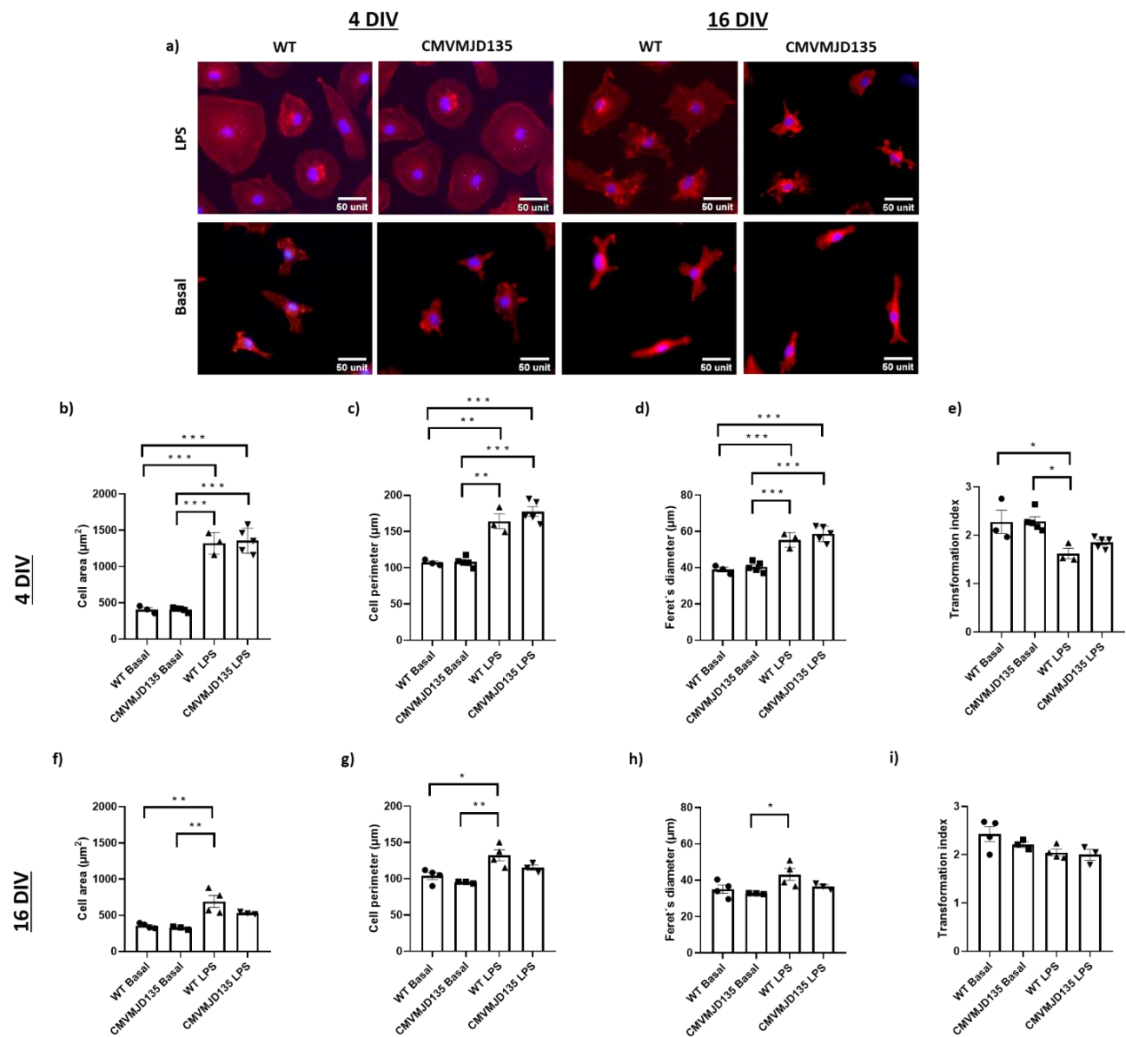
**Supplementary Figure S1. Purity assessment of microglia culture over time.** (a) Representative images of immunocytochemistry using Iba-1 as a microglial marker (in red) and glial fibrillary acid protein (GFAP) as an astrocyte marker (in green) over time. (b) At 4 days *in vitro* (DIV), a high purity was observed (98%), with a slight contamination with astrocytes occurring over time, but maintaining a 79% purity at 16 DIV. N = 3-4 independent experiments per each time point (4, 10, and 16 DIV). Each value represents the mean  $\pm$  SEM. Scale bar: 50  $\mu$ m.

**Evaluation of the expression levels of mutant human *ATXN3* in microglia**



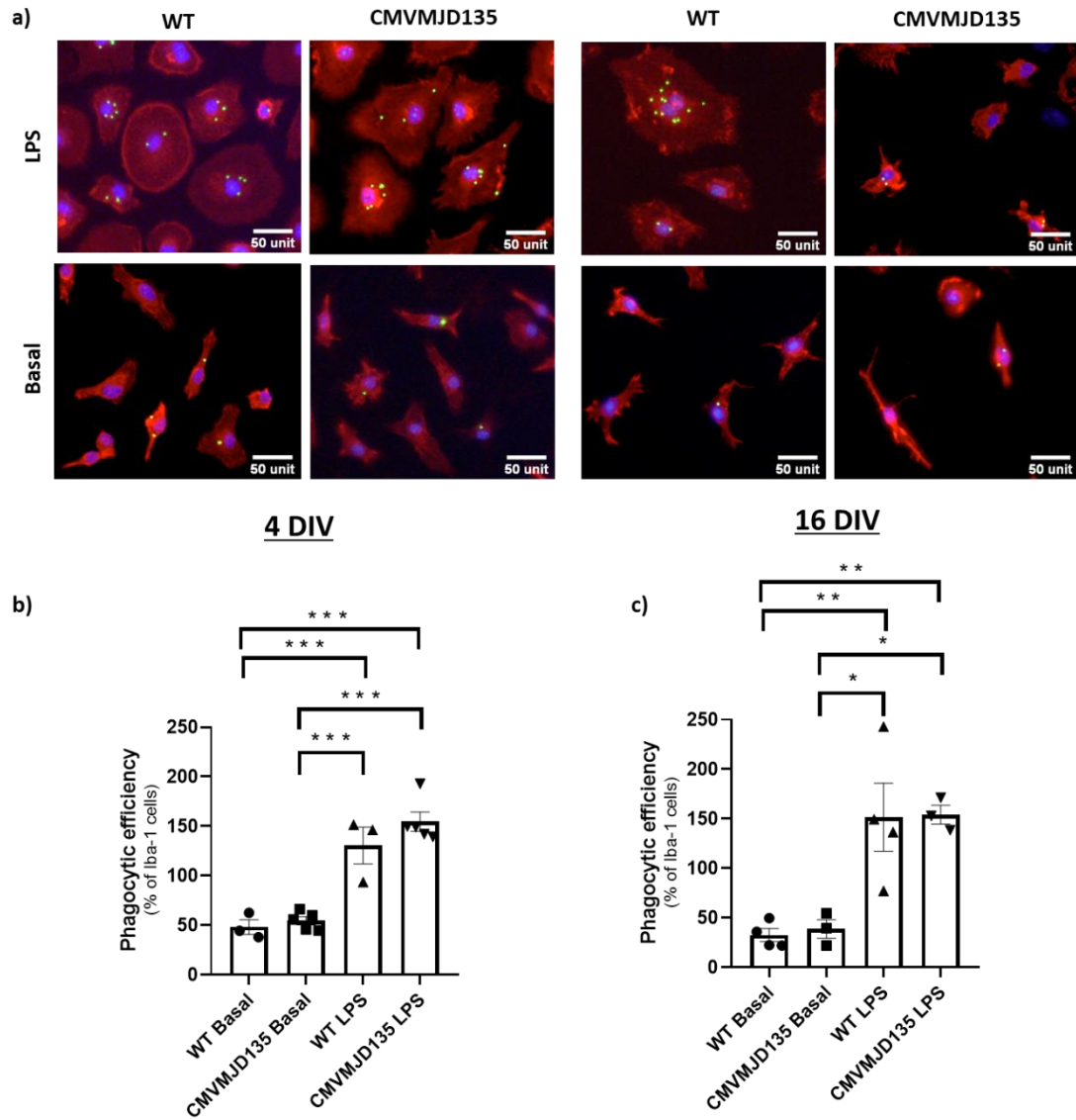
**Supplementary Figure S2. Expression of mutant *ATXN3* in microglia from CMVMJD135 mice at two different time points in culture.** a) at 4 DIV, and b) at 16 DIV. Cultures of  $n = 4-5$  animals per group. Two technical replicates were performed. Fold change ( $2^{-\Delta\Delta CT}$ ) is represented using mouse endogenous *Atxn3* as reference gene. Data are presented as mean+SEM (Student's t-test). \*, \*\*\*, represent  $p < 0.05$  and  $p < 0.001$ , respectively.

## Evaluation of microglial morphology in culture



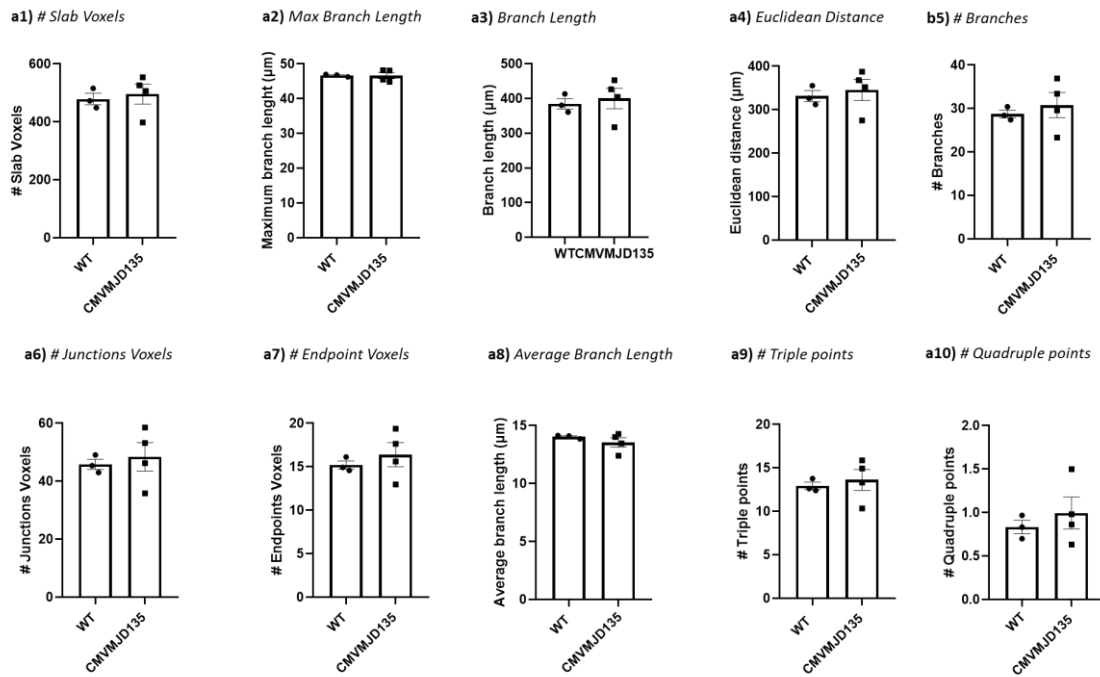
**Supplementary Figure S3. Microglia expressing *ATXN3* showed a less activated phenotype in response to lipopolysaccharides (LPS) in artificially “aged” primary cultures. a)** Images that represent the morphological changes of microglia, as observed by immunocytochemistry using microglia-specific marker Iba-1 (in red), from CMVMJD135 and Wild-Type (WT) mice, in the absence/presence of LPS, over time, in culture; **b-e)** cell area; **c)** cell perimeter; **d)** Feret's diameter; and **e)** transformation index. **b-e)** measured at 4 DIV; and **f-i)** measured at 16 DIV. Cultures of  $n = 3-5$  animals per group. Data are presented as mean+SEM, (One-way ANOVA (Post hoc Tukey's test)). \*, \*\*, \*\*\*, represent  $p < 0.05$ ,  $p < 0.01$  and  $p < 0.001$ , respectively. Scale bar unit as  $\mu\text{m}$ .

**Evaluation of microglia phagocytic ability in culture**



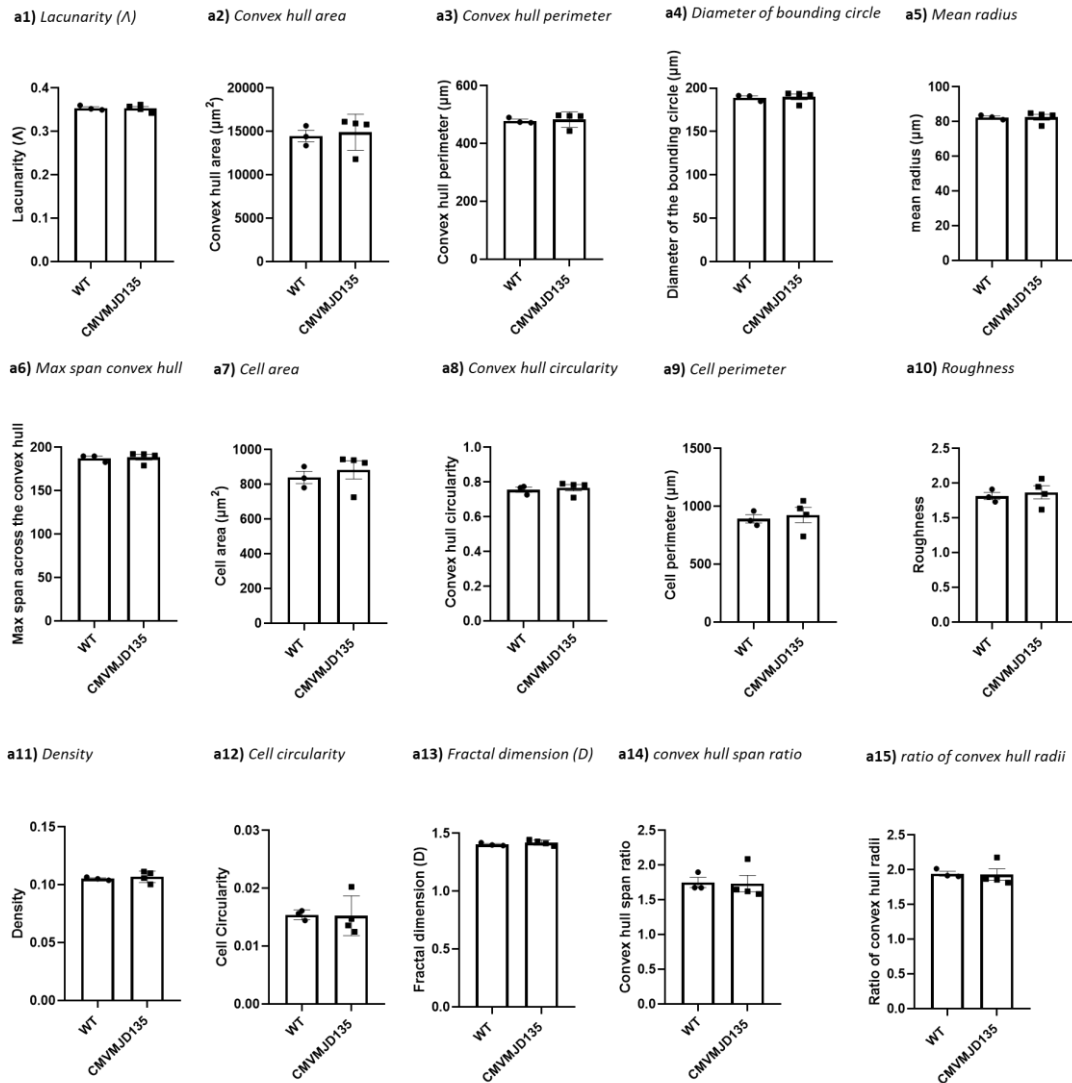
**Supplementary Figure S4. CMVMJD135 and WT-derived microglia showed an increased phagocytic efficiency in the presence of LPS in culture.** **a)** Representative images of the phagocytic capacity of CMVMJD135 and WT-derived microglia immunostained for Iba-1 (in red) and counterstained with 4',6-Diamidin-2-phenylindol (DAPI) for nuclei staining (in blue) containing phagocytosed fluorescent beads (in green), in the absence/presence of LPS, over time in culture. **b, c)** Phagocytic efficiency (%) was measured using ImageJ and calculated as previously described. Cultures of n = 3-5 per group. Data are presented as mean+SEM, (One-way ANOVA (Post hoc Tukey's test)). \*, \*\*, \*\*\*, represent  $p < 0.05$ ,  $p < 0.01$  and  $p < 0.001$ , respectively. Scale bar unit as  $\mu\text{m}$ .

## Morphological analysis of microglia from the PN of CMVMJD135 and WT mice



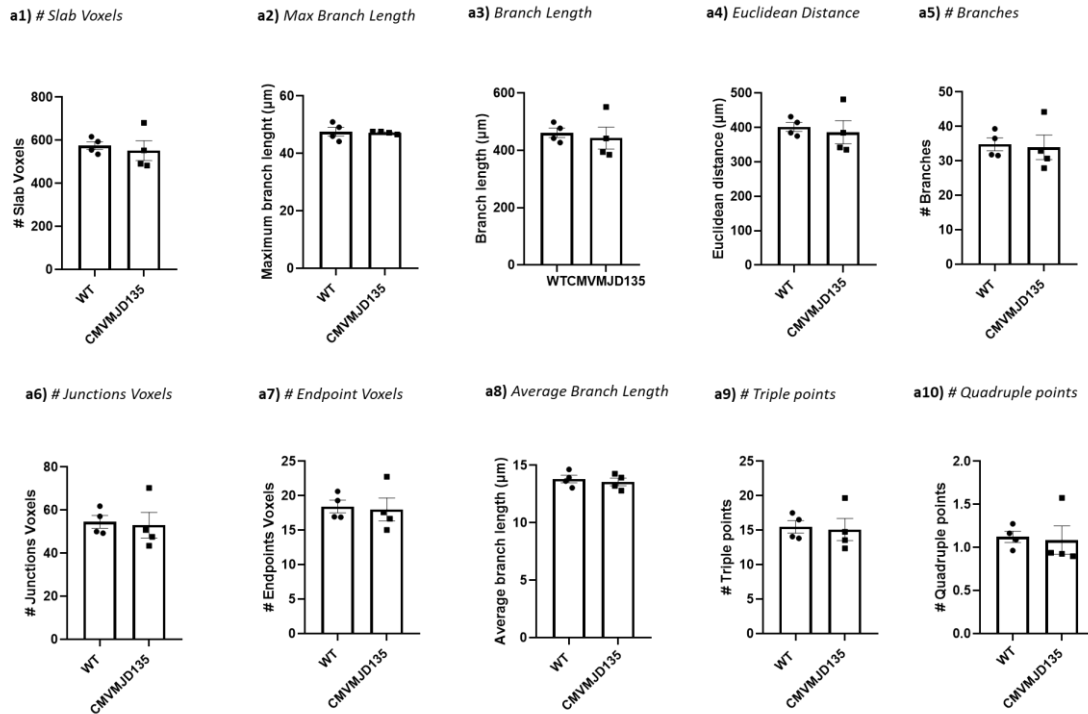
**Supplementary Figure S5. The ramification state of microglia in the pontine nuclei (PN) of the CMVMJD135 mice is similar to those of microglia from WT mice.** a) Quantification of the morphometric parameters associated with microglia ramification, including: **a1)** # slab voxels; **a2)** maximum branch length; **a3)** branch length; **a4)** Euclidean distance; **a5)** # branches; **a6)** # junctions' voxels; **a7)** # endpoints voxels; **a8)** average branch length; **a9)** # triple points; and **a10)** # quadruple points. Values for all these parameters were obtained from 152 microglial cells from WT mice (n = 3) and 180 microglial cells from CMVMJD135 mice (n = 4) of the PN. Data are presented as mean+SEM (Student's t-test).

## Morphological analysis of microglia from the PN of CMVMJD135 and WT mice



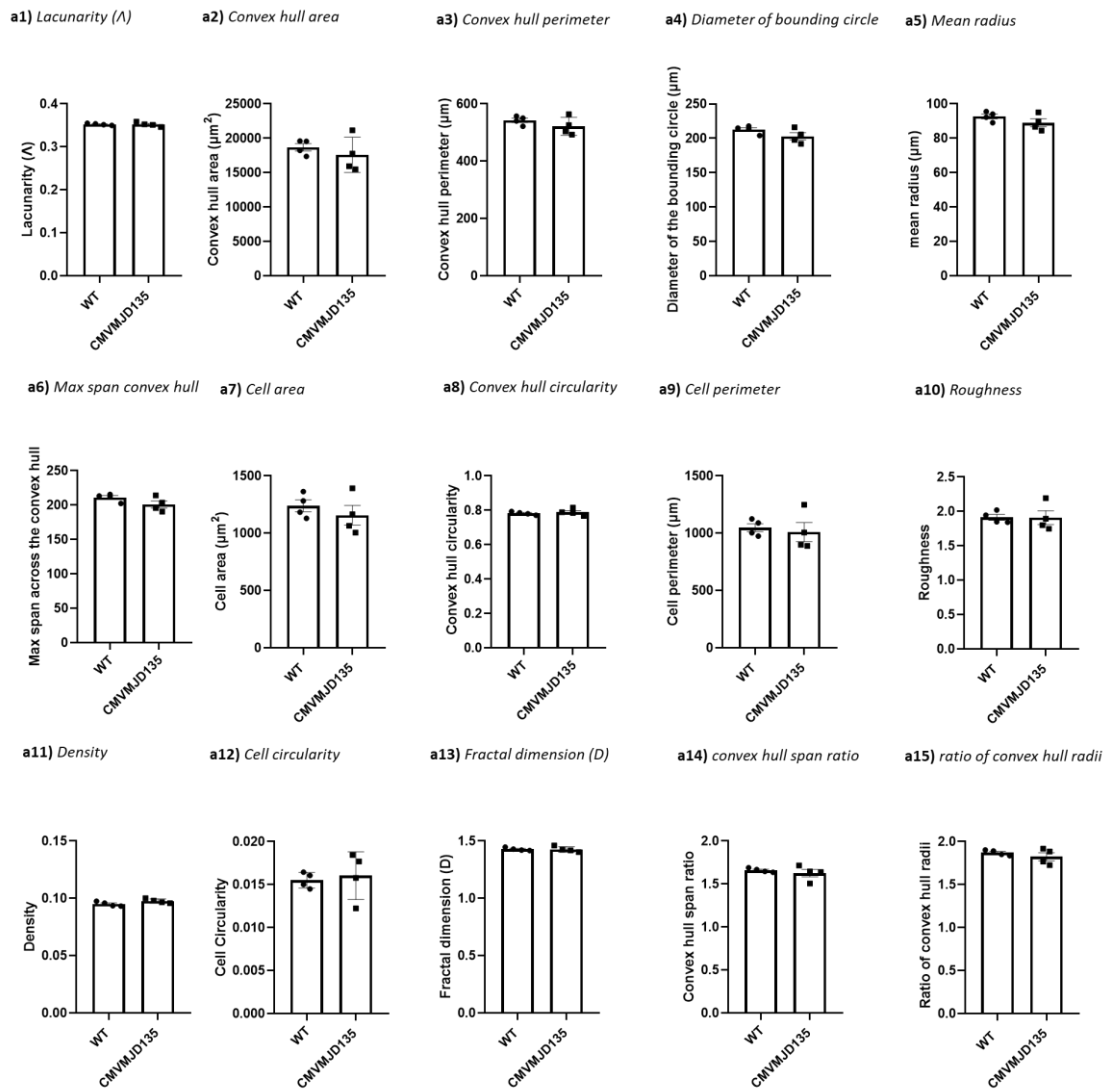
**Supplementary Figure S6. The complexity and shape of microglia in the PN of CMVMJD135 mice are similar to those of microglia from WT mice.** a) Quantification of the morphometric parameters associated with the heterogeneity of the shape: **a1)** lacunarity ( $\Lambda$ ); associated with cell size: **a2)** convex hull area, **a3)** the convex hull perimeter, **a4)** the diameter of bounding circle, **a5)** the mean radius, **a6)** the maximum span across the convex hull, **a7)** the cell area, and **a8)** the convex hull circularity; associated with cell surface **a9)** cell perimeter and **a10)** roughness; associated with soma thickness: **a11)** density and **a12)** cell circularity; associated with the complexity of ramifications: **a13)** fractal dimension (D); and associated with the cylindrical shape of cells: **a14)** convex hull span ratio and **a15)** the ratio of convex hull radii. Values for all these parameters were obtained from 152 microglial cells from WT mice ( $n = 3$ ) and 180 microglial cells from CMVMJD135 mice ( $n = 4$ ) of the PN. Data are presented as mean+SEM (Student's t-test).

## Morphological analysis of microglia from the DCN of CMVMJD135 and WT mice



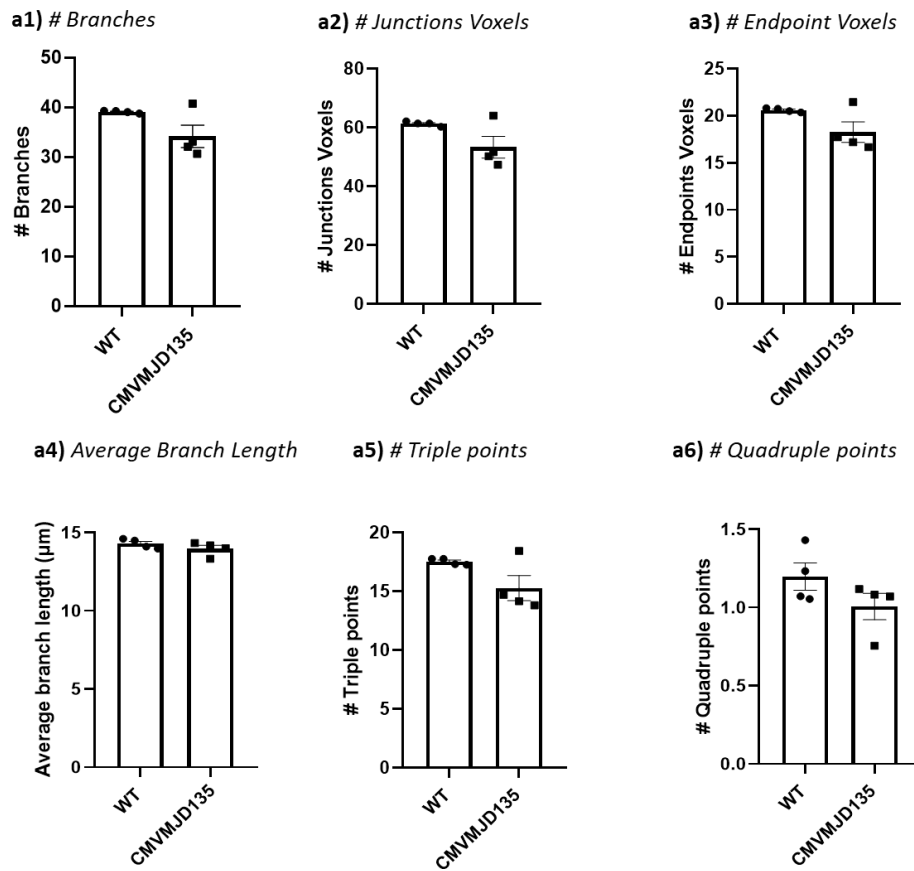
**Supplementary Figure S7. Microglia in the deep cerebellar nuclei (DCN) of CMVMJD135 mice showed no differences in features relevant to microglia ramification.** a) Quantification of the morphometric parameters associated with microglia ramification including: **a1)** # slab voxels; **a2)** maximum branch length; **a3)** branch length; **a4)** Euclidean distance; **a5)** # branches; **a6)** # junctions' voxels; **a7)** # endpoints voxels; **a8)** average branch length; **a9)** # triple points; and **a10)** # quadruple points. Values for all these parameters were obtained from 349 microglial cells from WT mice (n = 4) and 445 microglial cells from CMVMJD135 mice (n = 4) of the DCN. Data are presented as mean+SEM (Student's t-test).

## Morphological analysis of microglia from the DCN of CMVMJD135 and WT mice



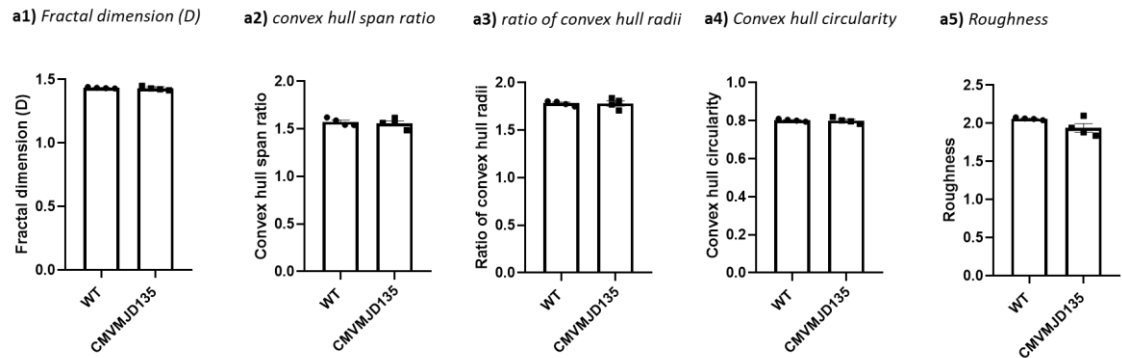
**Supplementary Figure S8. Microglia in the DCN of CMVMJD135 mice showed no changes in the complexity and shape.** **a)** Quantification of the morphometric parameters associated with heterogeneity of the shape: **a1)** lacunarity ( $\Lambda$ ); associated with cell size: **a2)** convex hull area, **a3)** the convex hull perimeter, **a4)** the diameter of bounding circle, **a5)** the mean radius, **a6)** the maximum span across the convex hull, **a7)** the cell area, and **a8)** the convex hull circularity; associated with cell surface: **a9)** cell perimeter and **a10)** roughness; associated with soma thickness: **a11)** density and **a12)** cell circularity; associated with the complexity of ramifications: **a13)** fractal dimension (D); and associated cylindrical shape of the cells: **a14)** convex hull span ratio and **a15)** the ratio of convex hull radii. Values for all these parameters were obtained from 349 microglial cells from WT mice ( $n = 4$ ) and 445 microglial cells from CMVMJD135 mice ( $n = 4$ ) of the DCN. Data are presented as mean+SEM (Student's t-test).

## Morphological analysis of microglia from the CSC of CMVMJD135 and WT mice



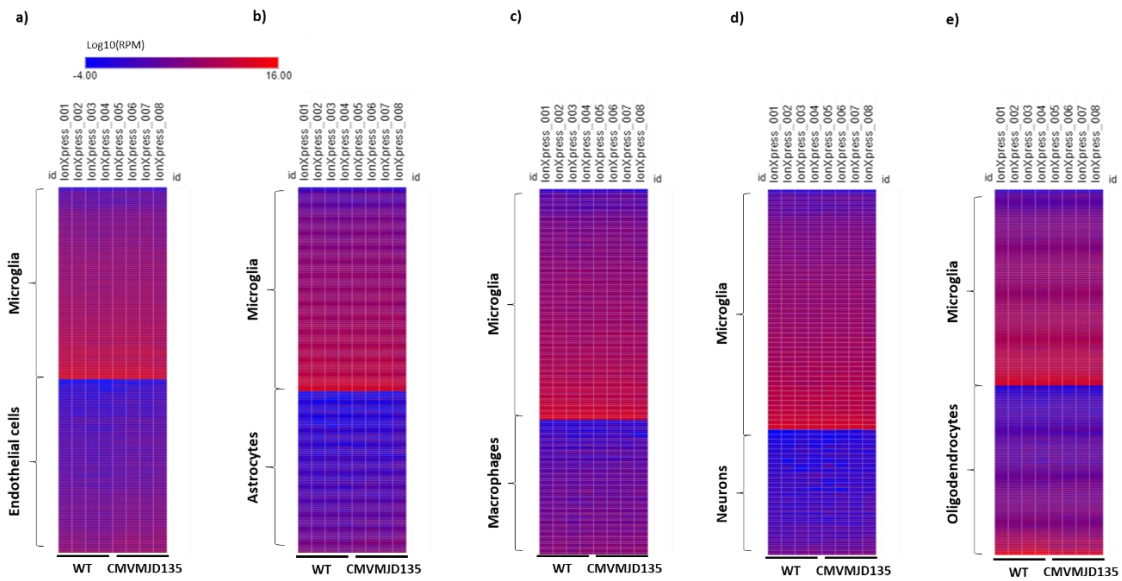
**Supplementary Figure S9. Some parameters associated with microglia ramification were similar between CMVMJD135 and WT mice in the cervical spinal cord (CSC).** a) Quantification of the morphometric parameters associated with microglia ramification including: **a1)** # branches; **a2)** # junctions' voxels; **a3)** # endpoints voxels; **a4)** average branch length; **a5)** # triple points; and **a6)** # quadruple points. Values for all these parameters were obtained from 310 microglial cells from WT mice ( $n = 4$ ) and 389 microglial cells from CMVMJD135 mice ( $n = 4$ ) of the CSC. Data are presented as mean+SEM (Student's t-test).

## Morphological analysis of microglia from the CSC of CMVMJD135 and WT mice



**Supplementary Figure S10. No changes were observed in the parameters related to the complexity of ramifications and with the cylindrical shape of the cells between groups in the CSC. a)** Quantification of the morphometric parameters associated with the complexity of ramifications: **a1)** fractal dimension (D); associated with cylindrical shape of the cells: **a2)** convex hull span ratio and **a3)** the ratio of convex hull radii; one of the parameters associated with cell's size: **a4)** the convex hull circularity; and one of the parameters associated with cell's surface: **a5)** roughness. Values for all these parameters were obtained from 310 microglial cells from WT mice (n = 4) and 389 microglial cells from CMVMJD135 mice (n = 4) of the CSC. Data are presented as mean+SEM (Student's t-test).

## Evaluation of microglial enrichment in samples from CMVMJD135 and WT mice



**Supplementary Figure S11. Evaluation of microglial enrichment in RNA-sequencing samples.** Heatmaps showing high levels of expression for specific markers of microglia when compared with markers of other cell-types. a) Microglia versus endothelial cells; b) microglia versus astrocytes; c) microglia versus macrophages; d) microglia versus neurons; and e) microglia versus oligodendrocytes. Four biological replicates for WT and CMVMJD135 mice were used. An heatmap containing the cell-specific markers was achieved using the Clue Morphheus software.

## RNA-sequencing analysis of microglia from CMVMJD135 and WT mice

a)

ID	Fold Chan...	P-val	FDR P-val	Public Gene IDs	Gene Symbol
count: 83					
Ufl1	1,72	1,63E-06	0,0097	NM_026194	Ufl1
Lrrc58	1,49	3,44E-06	0,0137	NM_177093	Lrrc58
Lamc1	2,5	4,34E-06	0,0149	NM_010683	Lamc1
Cdyl	1,95	8,26E-06	0,0247	NM_001123386	Cdyl
Rnf144b	1,54	1,37E-05	0,0364	NM_001170643	Rnf144b
Ncam1	2	1,55E-05	0,0367	NM_001081445	Ncam1
Ddb1	1,47	1,75E-05	0,0367	NM_015735	Ddb1
Cux2	2,36	1,84E-05	0,0367	NM_001312908	Cux2
A2m	1,97	2,29E-05	0,0391	NM_175628	A2m
Epsti1	1,28	3,46E-05	0,0552	NM_029495	Epsti1
Hipk3	1,71	3,88E-05	0,0581	NM_001145824	Hipk3
Ccdc151	2,36	4,16E-05	0,0581	NM_001163787	Ccdc151
Arhgef12	1,79	4,49E-05	0,0581	NM_027144	Arhgef12
Pcdhb21	2,83	4,77E-05	0,0581	NM_053146	Pcdhb21
Mef2c	1,43	5,24E-05	0,0597	NM_001170537	Mef2c
Mira	1,67	5,88E-05	0,0639	NR_045199	Mira
L3mbtl3	1,98	6,73E-05	0,0686	NM_172787	L3mbtl3
Fam188b	1,62	6,88E-05	0,0686	NM_001142781	Fam188b
Gm6548	2,33	7,64E-05	0,0697	NR_003363	Gm6548
Tmem136	2,02	7,78E-05	0,0697	NM_001034863	Tmem136
4930564C03Rik	1,72	7,86E-05	0,0697	NM_029257	4930564C03Rik
Pcnx3	1,82	0,0001	0,0817	NM_144868	Pcnx3
Scd2	1,74	0,0001	0,0817	NM_009128	Scd2
Haghl	1,48	0,0001	0,0817	NM_001271433	Haghl
Zfp568	2,01	0,0001	0,0850	NM_001033355	Zfp568
Ak8	1,98	0,0001	0,0850	NM_001033874	Ak8
Mpg	1,69	0,0001	0,0850	NM_010822	Mpg
Ap3m2	1,61	0,0001	0,0850	NM_001122820	Ap3m2
Sox8	2,07	0,0001	0,0850	NM_011447	Sox8
Rbbp6	1,56	0,0001	0,0850	NM_011247	Rbbp6

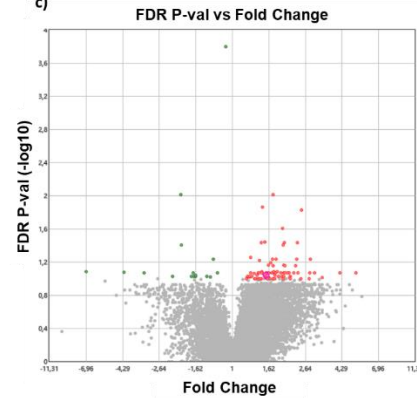
ID	Fold Chan...	P-val	FDR P-val	Public Gene IDs	Gene Symbol
count: 83					
Ptpn4	1,78	0,0001	0,0850	NM_019933	Ptpn4
Nav1	1,9	0,0002	0,0850	NM_173437	Nav1
Abcb1a	2,25	0,0002	0,0850	NM_011076	Abcb1a
Igfbp3	5,15	0,0002	0,0850	NM_008343	Igfbp3
Celsr1	2,81	0,0002	0,0850	NM_009886	Celsr1
Dok7	4,17	0,0002	0,0850	NM_172708	Dok7
Zc3h6	2,97	0,0002	0,0850	NM_178404	Zc3h6
Hydin	2,39	0,0002	0,0850	NM_172916	Hydin
Alpl	2,13	0,0002	0,0850	NM_001287172	Alpl
Abca7	1,7	0,0002	0,0850	NM_013850	Abca7
Syt3	1,48	0,0002	0,0850	NM_001114116	Syt3
St8sia4	1,63	0,0002	0,0850	NM_001159745	St8sia4
Gsk3b	1,59	0,0002	0,0850	NM_019827	Gsk3b
Acs14	1,41	0,0002	0,0850	NM_001033600	Acs14
Csad	1,27	0,0002	0,0850	NM_144942	Csad
Tanc1	1,43	0,0002	0,0850	NM_001290659	Tanc1
St5	1,5	0,0002	0,0867	NM_001001326	St5
Tmem106b	1,33	0,0002	0,0867	NM_027992	Tmem106b
Prrc2a	1,76	0,0002	0,0906	NM_001199044	Prrc2a
Kihl24	1,39	0,0002	0,0906	NM_029436	Kihl24
Sh2d5	1,56	0,0002	0,0906	NM_001099631	Sh2d5
Rad54l2	1,57	0,0002	0,0906	NM_030730	Rad54l2
Zfp882	1,26	0,0003	0,0930	NM_001166645	Zfp882
Degs2	2,15	0,0003	0,0930	NM_001171002	Degs2
Vps37c	1,3	0,0003	0,0930	NM_181403	Vps37c
Bmpr2	1,99	0,0003	0,0930	NM_007561	Bmpr2
Arhgap20	1,94	0,0003	0,0930	NM_175535	Arhgap20
Xpr1	1,23	0,0003	0,0930	NM_011273	Xpr1
Caskin2	1,85	0,0003	0,0934	NM_080643	Caskin2
Gpld1	1,55	0,0003	0,0935	NM_008156	Gpld1

ID	Fold Chan...	P-val	FDR P-val	Public Gene IDs	Gene Symbol
count: 83					
Ola1	1,27	0,0003	0,0954	NM_025942	Ola1
Foxf2	2,13	0,0003	0,0961	NM_010225	Foxf2
Cpd	1,62	0,0003	0,0961	NM_007754	Cpd
Cpsf7	1,63	0,0003	0,0961	NM_001164272	Cpsf7
1110004F10Rik	1,56	0,0003	0,0961	NM_019772	1110004F10Rik
Kat6a	1,22	0,0003	0,0961	NM_001081149	Kat6a
Mkl2	3,3	0,0003	0,0961	NM_001122667	Mkl2
Map3k19	1,64	0,0004	0,0995	NM_011737	Map3k19
Tyro3	2,17	0,0004	0,0995	NM_001290800	Tyro3
Fmnl2	1,59	0,0004	0,0995	NM_172409	Fmnl2
Atp2b4	1,72	0,0004	0,0995	NM_001167949	Atp2b4
Junb	1,45	0,0004	0,0995	NM_008416	Junb
Atp6v0a1	1,46	0,0004	0,0995	NM_001243049	Atp6v0a1
Atg101	1,41	0,0004	0,0995	NM_026566	Atg101
Frmd4b	1,36	0,0004	0,0995	NM_145148	Frmd4b
Cnot1	1,34	0,0004	0,0995	NM_001205226	Cnot1
Ahnak	1,97	0,0004	0,0995	NM_001039959	Ahnak
Arhgef15	2,48	0,0004	0,0995	NM_177566	Arhgef15
Ntn1	2,78	0,0004	0,0995	NM_008744	Ntn1
Fos	1,47	0,0004	0,0995	NM_010234	Fos
Rnh1	1,21	0,0004	0,0995	NM_001172100	Rnh1
Fbx12	1,76	0,0004	0,0995	NM_001002846	Fbx12
Stard13	2,16	0,0004	0,0995	NM_001163493	Stard13

b)

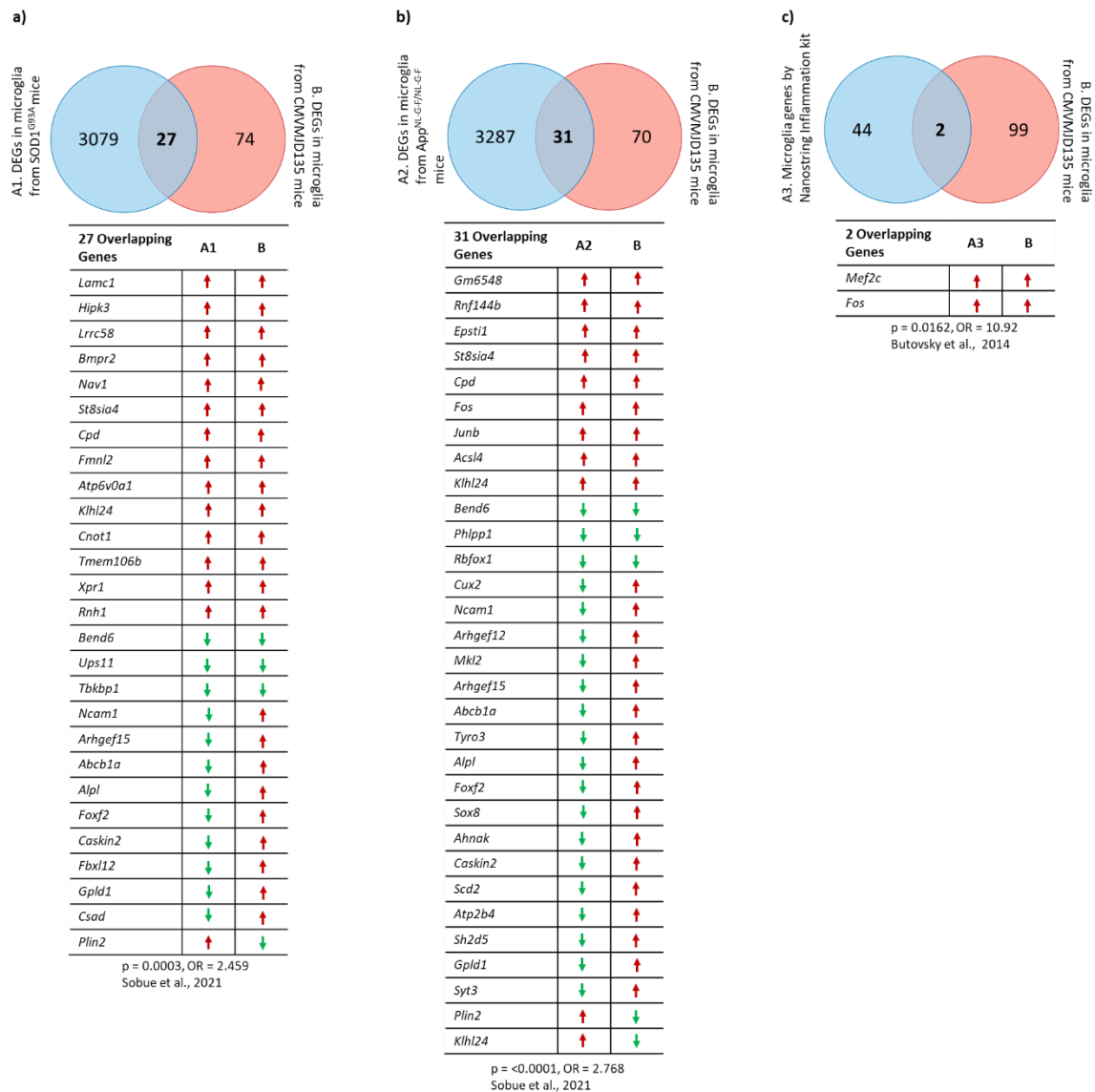
ID	Fold Chan...	P-val	FDR P-val	Public Gene IDs	Gene Symbol
count: 18					
4921530L21Rik	-1,09	1,98E-08	0,0002	NM_025733	4921530L21Rik
Cpsf1	-1,09	1,98E-08	0,0002	NM_001164173	Cpsf1
Olfir791	-1,09	1,98E-08	0,0002	NM_146930	Olfir791
Zfp62	-1,98	2,04E-06	0,0097	NM_001024846	Zfp62
Bend6	-1,97	2,16E-05	0,0391	NM_001310484	Bend6
Usp11	-1,28	4,85E-05	0,0581	NM_145628	Usp11
Gm2694	-6,97	9,62E-05	0,0817	NR_033430	Gm2694
LOC108169012	-4,19	0,0001	0,0841	XR_001784563	LOC108169012
Akap7	-3,22	0,0001	0,0850	NM_018747	Akap7
Fbxw4	-1,68	0,0002	0,0850	NM_013907	Fbxw4
Nek9	-1,22	0,0002	0,0850	NM_145138	Nek9
Hoxb8	-1,63	0,0002	0,0906	NM_010461	Hoxb8
Phlpp1	-1,67	0,0003	0,0930	NM_133821	Phlpp1
Plin2	-1,41	0,0003	0,0930	NM_007408	Plin2
Pnpla3	-1,63	0,0003	0,0930	NM_054088	Pnpla3
Rbfox1	-2,21	0,0003	0,0930	NM_021477	Rbfox1
Tasp1	-1,72	0,0003	0,0930	NM_001159640	Tasp1
Tbkbp1	-1,34	0,0003	0,0954	NM_198100	Tbkbp1

c)



**Supplementary Figure S12. Differential gene expression between microglial cells from CMVMJD135 and WT mice. a, b, c)** Up-regulated and down-regulated genes were determined using the Transcriptome Analysis Console (TAC) software, between CMVMJD135 and WT mice. **a)** Heatmap of 83 up-regulated genes in microglial cells from CMVMJD135 mice, in ascending order of False Discovery Rate (FDR) value. **b)** Heatmap of 18 down-regulated genes in microglial cells from CMVMJD135 mice, in ascending order of FDR value. **c)** Volcano plot view of CMVMJD135 versus WT genes. Red for up-regulated genes and green for down-regulated genes.  $|\text{fold change}| > 1$ ,  $p < 0.05$ , and an  $\text{FDR} < 0.1$  was considered to determine genes significantly differentially expressed.

## Transcriptional changes seen in CMVMJD135 microglia overlap those in Amyotrophic lateral sclerosis (ALS) and Alzheimer disease (AD) mouse models



**Supplementary Figure S13. Transcriptional changes seen in CMVMJD135 microglia overlap those in Amyotrophic lateral sclerosis (ALS) and Alzheimer disease (AD) mouse models.** Venn diagrams and table overview representing the overlapping genes between the 101 CMVMJD135-altered genes found in our RNA-sequencing analysis, with **a)** 3106 differentially expressed genes (DEGs) previously reported in the microglia of a mouse model of ALS, *SOD1<sup>G93A</sup>* mouse [51]; with **b)** 3318 DEGs previously reported in the microglia of a mouse model of AD, *App<sup>NL-G-F/NL-G-F</sup>* mouse [51]; and with **c)** 46 microglial genes highly expressed and/or affected in microglia in different neuroinflammatory conditions, as detected by the Nanostring inflammation kit [64]. Red arrows represent the up-regulated genes and green arrows represent the down-regulated genes. Comparisons were conducted by contingency analysis, using the Fisher's exact test and the Baptista-Pike method to calculate the odds-ratio. Significance was set at  $p < 0.05$ .

## 2. Supplementary References

[51] Sobue, A.; Komine, O.; Hara, Y.; Endo, F.; Mizoguchi, H.; Watanabe, S.; Murayama, S.; Saito, T.; Saido, T.C.; Sahara, N.; Higuchi, M.; Ogi, T.; Yamanaka, K. Microglial gene signature reveals loss of homeostatic microglia associated with neurodegeneration of Alzheimer's disease. *Acta Neuropathologica Communications* 2021, 9. doi:10.1186/s40478-020-01099-x.

[64] Butovsky, O.; Jedrychowski, M.P.; Moore, C.S.; Cialic, R.; Lanser, A.J.; Gabriely, G.; Koeglsperger, T.; Dake, B.; Wu, P.M.; Doykan, C.E.; Fanek, Z.; Liu, L.; Chen, Z.; Rothstein, J.D.; Ransohoff, R.M.; Gygi, S.P.; Antel, J.P.; Weiner, H.L. Identification of a unique TGF- $\beta$ -dependent molecular and functional signature in microglia. *Nature Neuroscience* 2014, 17, 131–43. doi:10.1038/nn.3599.